Steel and Composite Structures, *Vol. 19, No. 3 (2015) 547-567*
DOI: http://dx.doi.org/10.12989/scs.2015.19.3.547

Seismic behavior of rebar-penetrated joint between GCFST column and RGC beam

Guochang Li [1a], Chen Fang [*2], Yuwei An [1b] and Xing Zhao [1]

[1] *School of Civil Engineering, Shenyang Jianzhu University, 9 Hunnan East Road, Shenyang, Liaoning 110168, P.R. China*
[2] *Department of Civil Engineering, University of Texas at El Paso, 500 W. University Ave., El Paso, TX 79968, USA*

(*Received June 24, 2014, Revised January 27, 2015, Accepted January 31, 2015*)

Abstract. The paper makes the experimental and finite-element-analysis investigation on the seismic behavior of the rebar-penetrated joint between gangue concrete filled steel tubular column and reinforced gangue concrete beam under low cyclic reversed loading. Two specimens are designed and conducted for the experiment to study the seismic behavior of the rebar-penetrated joint under cyclic loading. Then, finite element analysis models of the rebar-penetrated joint are developed using ABAQUS 6.10 to serve as the complement of the experiment and further analyze the seismic behavior of the rebar-penetrated joint. Finite element analysis models are also verified by the experimental results. Finally, the hysteretic performance, the bearing capacity, the strength degradation, the rigidity degradation, the ductility and the energy dissipation of the rebar-penetrated joint are evaluated in detail to investigate the seismic behavior of the rebar-penetrated joint through experimental results and finite element analysis results. The research demonstrates that the rebar-penetrated joint between gangue concrete filled steel tubular column and reinforced gangue concrete beam, with full and spindle-shaped load-displacement hysteretic curves, shows generally the high ductility and the outstanding energy-dissipation capacity. As a result, the rebar-penetrated joint exhibits the excellent seismic performance and meets the earthquake-resistant requirements of the codes in China. The research provides some references and suggestions for the application of the rebar-penetrated joint in the projects.

Keywords: gangue concrete filled steel tube; joint; reinforced gangue concrete beam; seismic behavior; energy dissipation; ductility

1. Introduction

It is acknowledged in the industry that the concrete filled steel tubular (CFST) structure is an economy and effective composite system (Han *et al*. 2001). The regular concrete filled in the tube is replaced by the gangue concrete to develop a new and promising composite structure, the gangue concrete filled steel tubular (GCFST) structure (Li *et al*. 2012). Since the apparent density of the gangue concrete is less than the normal concrete, the weight of the GCFST structure

*Corresponding author, Ph.D. Student, E-mail: chenleofang@gmail.com
[a] Professor, E-mail: liguochang0604@sina.com
[b] Master Student, E-mail: 453109401@qq.com

Copyright © 2015 Techno-Press, Ltd.
http://www.techno-press.org/?journal=scs&subpage=8 ISSN: 1229-9367 (Print), 1598-6233 (Online)

presents a twenty percent reduction (Guo 2011). Another important merit of the GCFST structure is shown due to the better lateral deformation characteristic of the gangue concrete than the regular concrete. It gives full play to the confinement effect of the steel tube on the gangue concrete, which is conducive to the improvement of the bearing capacity of the composite structure (Li *et al*. 2010). Therefore, the GCFST structure has its own unique advantages and also exhibits the features of the favorable ductility and the large strength which the CFST structure shows. Moreover, with the development of the technology and economy, the green building has been a trend in the field of civil engineering (U.S. Environment Protection Agency 2009). As a non-recyclable industrial waste, the gangue is used for the structures. This can reduce the environmental pollution and achieve the economic and social benefits (Sun and Li 2011).

In the seismic design, it is the joint between the column and the beam that plays an essential role in ensuring the safety of the building under the severe earthquake (Krawinkler 1978). According to the design codes, the joint should be strong enough to form a hinge in the connection beam and maintain the ability to generate the bending capacity. In recent times, many researches have been done on the behavior of the joint between the CFST column and the beam. Varma *et al*. (2002) made an experimental study on the seismic performances of 16 joints between concrete filled steel square tubular column and steel beam under the reversed loading. Some parameters, such as the steel strength and the axial load level, were changed to determine the important factors influencing on the behavior of the joint. Choi *et al*. (2006) made the finite element analysis on the behavior of the joint between CFST column and steel beam with outside annular plate and analyzed the effects of main parameters on M-θ curve. Yiyan Chen (Yao *et al*. 2010, 2011) proposed a new type of the joint between CFST column and reinforced concrete (RC) beam and then analyzed the failure process, the failure mode and the energy dissipation of the joint by using the experiment and the finite element analysis. Chen *et al*. (2004) made a research on the stiffness of the joint between CFST column and steel beam with stiffening ring based on the finite element analysis and the experiment. It is clear that, most researches focus on the behavior of the joint between CFST column and steel beam. However, in China, the columns are often connected to the reinforced concrete beams in the real structural system. Few researches are attempted to study the behavior of the joint connected to the RC beam (Zhong 2003). Especially, data is still rare to investigate the behavior of the joint between GCFST column and reinforced gangue concrete (RGC) beam. Due to inadequate understanding of the behavior of the joint between GCFST column and RGC beam, the joint does not reach its full potential in this application.

As a result, the paper proposes a new type of joint between GCFST column and RGC beam and it is regarded as a typical rebar-penetrated joint. The specimens of the joint are fabricated for the experiment which is to investigate the seismic behavior of the joint. Then, finite element analysis models corresponding to experimental specimens are created using ABAQUS 6.10 to be the complement of the experiment. The finite element analysis models are verified with the experimental results. Finally, the seismic behaviors of the rebar-penetrated joint including the bearing capacity, the strength and rigidity degradation, the ductility and the energy dissipation are analyzed in the research.

2. Experiment

2.1 Design of specimens

Two joints between GCFST column and RGC beam are tested under the axial force in the top of the column and cyclic loads in the ends of the beams. The prototype ot the joint between GCFST column and RGC beam is designed referencing the requirements from the CECS28:2012 (2012) code. A new type of joint between GCFST column and RGC beam, which can be regarded as a typical rebar-penetrated joint, is designed and conducted in the research. In the joint, four holes are punched on the tube wall in the region of the joint. The longitudinal rebar embedded in the RGC beam is penetrated the column through the holes to transfer the bending moments. Owing to the holes in the tube which may reduce the bearing capacity of the joint, two strengthening rings are designed and welded below the holes. The stiffening ribs are also installed on both sides of the holes. The dimensions of the strengthening ring and the stiffening ring are determined based on the code for design of steel structures GB50017-2003 (2004). The code for design of concrete structures GB50010-2010 (2011) is used to design the size of the RGC beam and the dimension of the rebar. In the experiment, the specimens are designed and created as the exterior joint with one beam and the interior joint with two beams. The column is modeled as the circular gangue concrete filled steel tubular column. Due to the limitation of the experimental equipment, the axial load level of 0.6 is designed for the testing specimens.

According to the code for seismic design of buildings GB5011-2010 (2010), the specimens are designed with the characteristics of "strong column and weak beam". The primary purpose of the research is to investigate the seismic behavior of the composite joint subjected to the cyclic loading. Thus, the reinforced gangue concrete beam is designed to collapse under the earthquake, but the column should be extremely strong to resist the earthquake. This principle can ensure the safety and stability of the structure under the earthquake.

Table 1 Dimension of the specimen

Specimen Label	Column section dimension		Beam section dimension		Longitudinal rebars	Stirrup	N_0 (kN)	n
	$D\times t$ (mm)	H (mm)	$b\times h$ (mm)	L (mm)				
J6-E-B	325×6	1500	240×300	1000	1Φ20	ϕ10@100	1800	0.6
J6-E-Z	325×6	1500	240×300	2000	1Φ20	ϕ10@100	1800	0.6

Table 1 presents the summaries of the rebar-penetrated joint specimens. In the table, D represents the outside diameter of the GCFST column. t is the wall thickness of the steel tube. H is the height of the GCFST column. b is the width of the RGC beam. h is the height of the RGC beam. L represents the length of the RGC beam. n_0 is the axial load level in the column defined as $n_0 = N_0/N_u$, where N_0 is the axial load applied in the top of the column, N_u is the axial compressive capacity of the GCFST column according to the CECS28:2012 (2012) code. The mechanics mode proposed by Han and Huo (2003) for CFST columns is used to compute N_u in the research.

The details of the rebar-penetrated joint specimens are shown in Fig. 1. The specimens include the exterior joint and the interior joint. In these joints, the longitudinal rebar is designed to pass through the GCFST column. In the meanwhile, the strengthening ring and the stiffening ring are welded on the column to compensate for the decrease of the bearing capacity resulted from the holes. The rebar-penetrated joint specimen before the experiment is presented in Fig. 2.

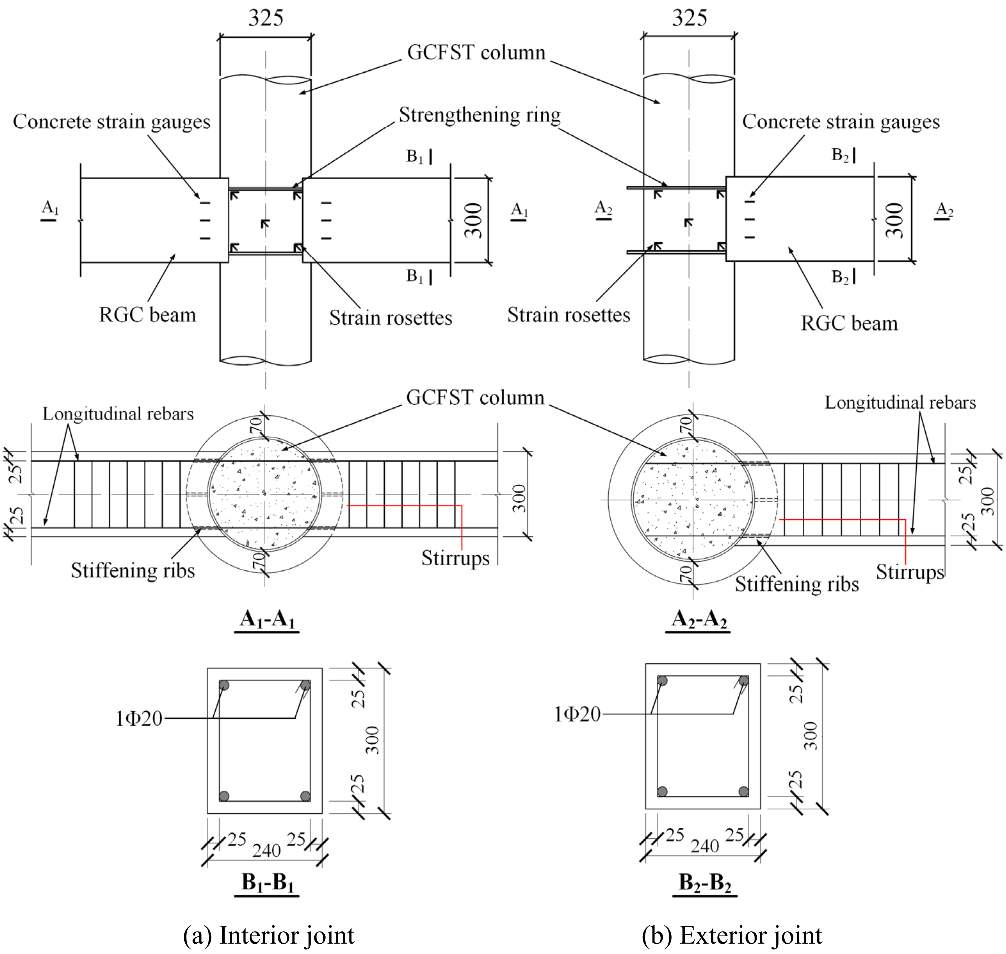

Fig. 1 Configuration of the joint specimens (mm)

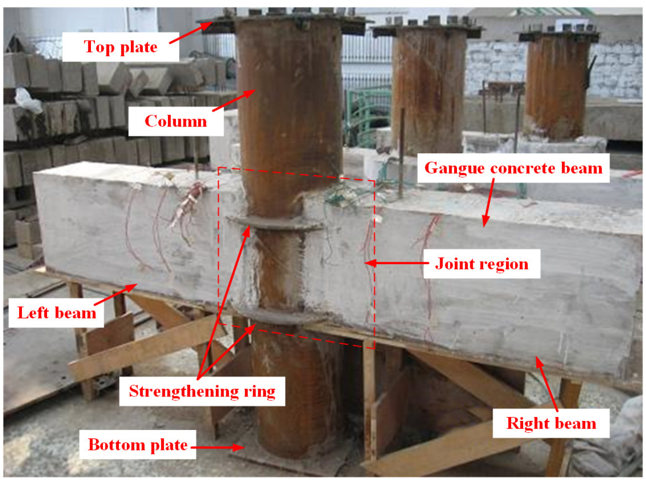

Fig. 2 Rebar-penetrated joint specimen before the experiment

Table 2 Material properties of steel

Steel types	Yield strength f_y (MPa)	Ultimate strength f_u (MPa)	Elastic modulus E (MPa)
Φ20 steel bar	411	524	2.17×10^5
ϕ10 steel bar	342	435	2.06×10^5
Steel plate with a thcikness of 8 mm	306	417	2.22×10^5
Steel plate with a thcikness of 6 mm	324	459	2.19×10^5

2.2 Material properties

The material properties of steel sheets and rebars are determined by the tension test referencing the recommendations from GB/T228-2002 (2003). Table 2 lists the measured average yield strength (f_y), the ultimate strength (f_u) and the elastic modulus (E).

The same gangue concrete is applied in fabrication of the GCFST column and the RGC beam. The gangue concrete mix proportion designed by the weight is including, the cement: 420 kg/m^3; the sand: 412.5 kg/m^3; the gangue: 412.5 kg/m^3; the coarse aggregate: 608 kg/m^3; and water: 250 kg/m^3.The regular portland cement with the grade of 32.5 and the coal gangue with the aggregate size of 5~20mm produced in Fuxin city are used to produce the gangue concrete. The compressive cube strength test is conducted for the gangue concrete block at 28 days according to the GB/T50081-2002 (2003) code. The average cube strength of the gangue concrete is 35.6 MPa. The elastic modulus of the gangue concrete is measured as 20100 MPa.

2.3 Loading apparatus and measurements

A general view of the experiment setup is shown in Fig. 3. A constant axial load (N_0) generated by a hydraulic jack is applied in the top of the column. The top and bottom of the column are

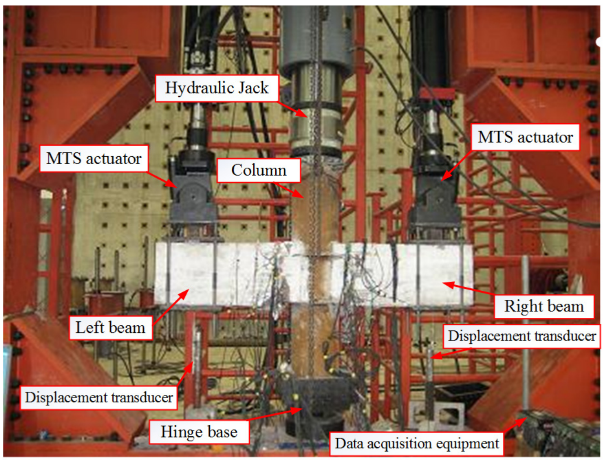

Fig. 3 General view of the experiment setup

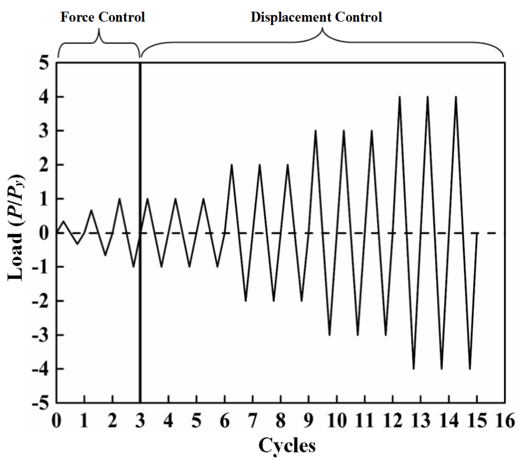

Fig. 4 Cyclic loading history

restrained to move horizontally, but are able to rotate in the loading plane. Two MTS hydraulic rams are set at the ends of two beams to simulate the cyclic loads in the vertical direction.

Fifty percentage of the axial load (N_0) is applied at the begining of the test to eliminate the heterogeneity of the materials. Then the axial load is increased to the designated value, and then keeps unchanged during the whole process of testing. The cyclic load with small increments is applied at the ends of both beams in the vertical direction, which is determined according to JGJ 101-96 (1997). A force control stage and a displacement control stage are included in the loading process of the cyclic load, shown in Fig. 4.

In the force control stage, one cycle is applied at the load levels of $0.33P_y$, $0.66P_y$ and P_y in the ends of both beams, respectively. P_y is the estimated yield load of the joint under bending moment and received from the finite element analysis model. In these joint specimens, P_y is close to the yield strength of the reinforced gangue concrete beam. When the cyclic load reaches P_y, the joint can be regarded as to be yielded. The displace control is applied as the vertical cyclic load in the ends of both beams. In the displacement control stage, the beams are subjected to the cycles of the displacement with the value of Δ_y, $2\Delta_y$, $3\Delta_y$, $4\Delta_y$, ..., respectively. Δ_y represents the yield displacement corresponded to the yield load P_y. Three cycles are imposed at each displacement level until the joint is collapsed. During the process of testing, the actuator is controlled at a rate of about 1kN/s in the force control stage. A rate of 1 mm/s is used for the displacement control stage.

The loads at the ends of both beam are meaured by the transducers inside MTS hydraulic actuator and the displacements are measured by displacement transducers located at the ends of the beams. A displacement transducer is set at the top of the column to measure the displacment of the column. Another two displacement transducers are used to measure the rotations of the GCFST column and RGC beam. Strain gauges are used to measure the strains of the steel tube, rebars and gangure concrete.

2.4 Experimental results

2.4.1 Specimen J6-E-Z

In the beginning of testing, it is in the force control stage and the deformation of the specimen shows the elastic characteristics. When fifty percent of the yield load (P_y) is reached, the first crack in a width of approximately 0.03 mm caused by bending moment is shown at the top or bottom surface of RGC beams. Then the crack is developing along the diagonal direction under the cyclic load. Displacements in ends of both beams, the strain of the steel tube and the strain in the rebar are small, demonstrating that the rebar-penetrated joint is working in the elastic stage. With the increasing cyclic loading, new cracks are observed and existing cracks are extending upon further loading. When the yield load is reached, the longitudinal rebar is yielded at the plastic hinge locations under the action of bending moment and shear force. At this point, an oblique crack with the width of 0.3 mm is found along the diagonal direction in the RGC beam.

After the yield load, the displacement control is to impose the cyclic load in the ends of both beams. New cracks are presented continually in the RGC beam with the increase of the cyclic load. When the longitudinal rebar is yielded, the widths of the cracks at this stage do not exceed the maximum value specified in the GB50010-2010 (2010) code on concrete structures. As the rebar-penetrated joint enters into the ultimate stage, it is clear that, the cracks are interlaced with each other in the region of the joint. The widths of the cracks further increase and the maximum width of the crack is larger than 1 mm. The shear deformation in the region of the joint is increased clearly. The deflection of beams was observed apparently. After the ultimate stage, the

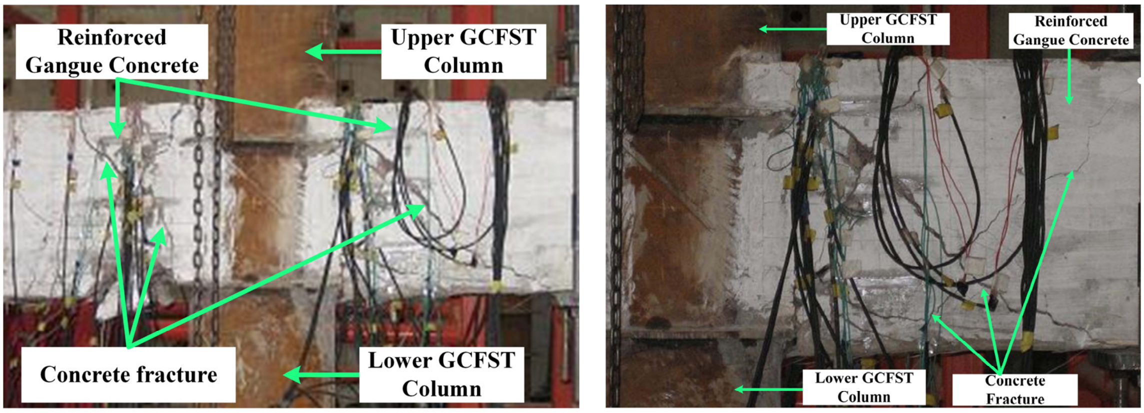

Fig. 5 Failure modes of the specimen J6-E-Z

load bearing capacity of the joint reduces quickly and the damage of the gangue concrete in the beam is aggravated. An extremely wide crack passed through the depth of the beam is located in the part of the RGC beam in which it is connected with the strengthening rings. The concrete cover of the beam is spalling at the joint, but the performance of the joint is not affected significantly by the spalling of concrete. Finally, when the baring capacity of the joint is reduced to less than eighty-five percent of the ultimate bearing capacity, the test is terminated. The failure modes of the specimen J6-E-Z are shown as Fig. 5.

2.4.2 Specimen J6-E-B

In the force control stage at the beginning of testing, the deformation of the specimen presents the elastic characteristics. When the cyclic load reaches 48.2 kN, the first crack in a width of approximately 0.03 mm is shown at the top or bottom surface of RGC beams. With the increase of the cyclic load, the crack develops and expands. When the cyclic load reaches 90 kN, an oblique crack passed through the depth of the beam is found along the diagonal direction. The crack continues developing with the increase of the cyclic load. When the cyclic load is 110 kN, the longitudinal rebar is yielded and the displacement corresponding to the yield load is defined as the yield displacement of the specimen. At this moment, the test turns to be in the displacement control stage. As the number of the cycle increases, new cracks are appeared in the RGC beam. Existing cracks are expanding and developing and the widths of these cracks are increasing. At the cyclic displacement of Δ_y, the cracks are expanded to interlace with each other. As the cyclic displacment increases to $2\Delta_y$, bidirectional diagonal cracks are observed on the core part of the jiont zone. When the cyclic displacement reaches $3\Delta_y$, the cracks develop from the top and bottom of the beams together at the plastic hinge loacation and a wide crack passed through the depth of the beam is formed obviously. After the penetrated crack is formed, the load of the joint gradually increases to the ultimate load bearing capacity. The diagonal cracks in the zone of joint become wider and apparent deflection of the beam can be observed. After the peak load, the load-bearing capacity of the joint decreases gradually. The concrete cover of the beam is flaking, but the performance of the joint is not affected significantly by the spalling of concrete. Finally, when the baring capacity of the joint is reduced to less than eighty-five percent of the ultimate bearing capacity, the test is terminated. The failure modes of the specimen J6-E-B are shown in Fig. 6.

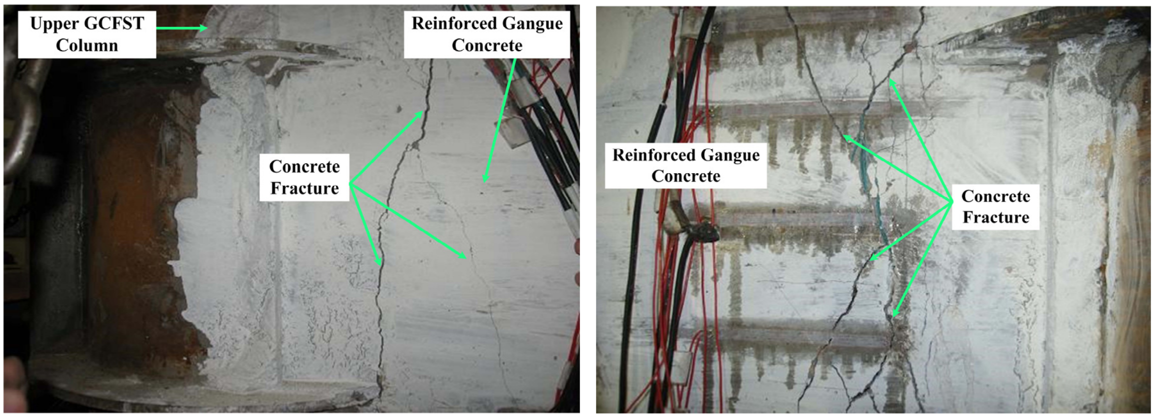

Fig. 6 Failure modes of the specimen J6-E-B

3. Finite element analysis model

Owing to the limitation of the experiment, finite element analysis models are designed and created in the research to be the supplement. According to the experimental specimens, the axial load level is changed to develope different models and further investigate the effec of the axial load level on the seismic behavior of the rebar-penetrated joint between GCFST column and RGC beam.

3.1 Material constitutive model

3.1.1 Gangue concrete

In order to simulate reasonably stiffness deterioration of the concrete, the concrete plastic damage model provided by ABAQUS 6.10 is used to simulate the concrete material (Yu *et al*. 2010). For the compressive zone of the gangue concrete filled in the tube, owing to the constraint effect of tube on the gangue concrete, the gangue concrete is subjected to three-dimensional compressive stress. So the stress-strain relationship curve of the light aggregate concrete filled in steel tube proposed by Fu *et al*. (2011) is applied to simulation on the property of the gangue concrete filled in tube. For the compressive zone of the unrestrained gangue concrete, the stress-strain relationship curve of light aggregate concrete provided by Southeast University (Zhang and Cao 2009) is used, shown in Fig. 7. Because this relationship curve can make the computation easy to converge and also finite element analysis results computed by using the model conform well with the experimental results. The energy fracture criterion (Sorenson 2003) can define the softening property of the concrete and enhance the convergence of computation. Hence, the fracture energy (G_f)-crack displacement relation curve is chosen to simulate the property of the gangue concrete in the tensile zone, shown in Fig. 8. In order to correspond to the experiment, the average cube strength of the gangue concrete is defined as 35.6 MPa. The elastic modulus of the gangue concrete is defined as 20100 MPa. The evolution of the compressive damage variable (d_c) is introduced to represent the damage of the concrete. The stress-strain relationship under uniaxial compressive loading is formulated as follows

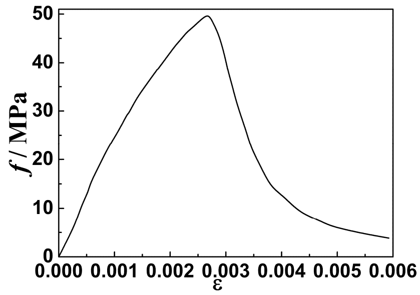

Fig. 7 Constitutive model of unrestrained concrete

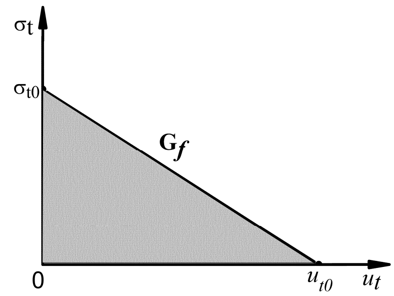

Fig. 8 Fracture energy-crack displacement relation curve

$$d_c = 1 - \frac{(\sigma_c + n_c\sigma_{cu})}{E_c(\frac{n_c\sigma_{cu}}{E_c} + \varepsilon_c)} \tag{1}$$

where σ_c is the compressive stress on the material; σ_{cu} is the ultimate compressive strain; E_c is the elastic stiffness of concrete; ε_c is the compressive strain; n_c is the constant factors for compression and should be larger than 0. Through extensive trials and experience, $n_c = 2$ is taken for the confined gangue concrete in GCFST column under compression. $n_c = 1$ is taken for the unconfined gangue concrete in GC beam. The default of the compressive stiffness recovery factor w_c is taken as 0 in the computation.

3.1.2 Steel

For the steel of tube and strengthening ring, the stress-strain relationship curve of steel under cyclic loading (Han 2000) is applied, shown in Fig. 9. In addition, as Bauschinger effect (Li and Zhao 2003) has an important influence on the bearing capacity of the structure, the Kinematic Hardening model with a von Mises yield surface (Boger 2006) is applied in the constitutive model of steel. On the basis of many trials and previous researches, the double linear model with bearing capacity deterioration (USTEEL02) in the hysteretic constitutive model collection (PQ-Fiber) proposed by Tsinghua University (Lu *et al*. 2009) is used to simulate on the property of the rebar embedded in the gangue concrete beam. The model (USTEEL02) can present the hysteretic behavior of the rebar under cyclic loading and simulate the bond slip between rebar and gangue concrete. In the meanwhile, this model is easy to ensure the convergence of the computation and the accuracy of the finite element analysis results. In order to simplify the finite element analysis model, the yield strength of the steel is defined as 325 MPa and the elastic modulus is defined as 2.06×10^5 MPa. The Poisson's ratio is set to 0.3.

3.2 Element and mesh

The 8-node brick element with reduced integration (C3D8R) is used as the element model to create the gangue concrete. The mapping self-customized meshing is chosen to mesh the gangue concrete. The continuous shell element is used for the steel and the type of element is the four-node conventional shell element with reduced integration (S4R). Truss element is applied to emulation of the rebar embedded in the beam. Fig. 10 shows the finite element analysis model

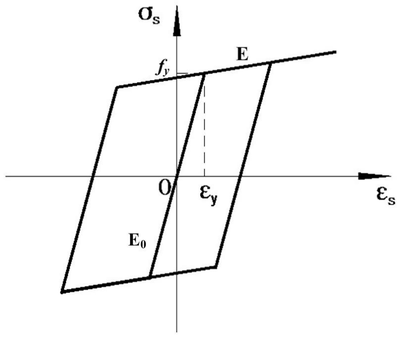

Fig. 9 Stress-strain relation of steel

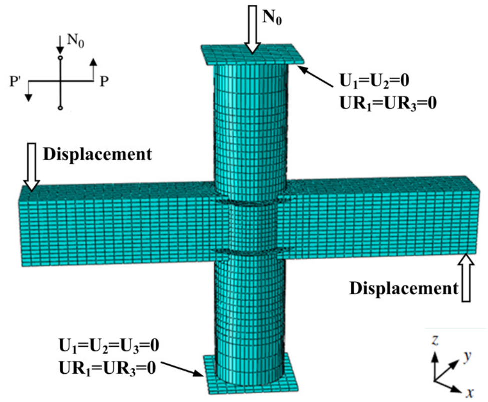

Fig. 10 Analysis model of rebar-perforated joint

of the rebar-penetrated joint. In order to be same as boundary conditions in the experiment, all degrees of freedom except the rotation around y axis in the bottom of the column are constrained. The displacements in *x*, *y* direction and the rotations around *x*, *z* axes in the top of column are constrained to simulate the pinned joint. During the process of computation, the concentrated force is applied in the top of the column and two displacements with the same magnitude but the opposite direction are applied on both beam ends.

The accuracy and reasonability of finite element analysis models depends on the proper mesh density. The mesh size in the core part of the ring beam joint is refined and the meshing density in other parts is relatively increased, which is helpful to ensure the accuracy of the computation and accelerate the computation speed. The mesh sizes of the steel tube and the gangue concrete filled in the tube should be identical to make the computation convergence easy. The typical element discretization of the joint is shown in Fig. 10.

3.3 Contact model

The contact model between tube and core gangue concrete is composed of the contact in the normal direction and in the tangential direction. Hard contact is adopted to simulate the contact in the normal direction so as to transfer fully the compressive stress between the contact surfaces. Coulomb friction model (Hu *et al*. 2005) is applied to simulation of the tangential force. In the model, the penalty friction formula with the elastic slip is used to compute the tangential force. The friction coefficient between the steel and gangue concrete column is taken as 0.6. As the plate in the top and bottom of the column only transfers the compressive stress in the normal direction, the plate is assumed as elastic plate with large stiffness to simulate the bases. The elastic modulus is defined as 1×10^{12} MPa and Possion's ratio is 0.0001. The shell-to-solid coupling is used to simulate the contact model between the plate and tube, while the hard contact is applied to contact model between the plate and gangue concrete filled in the tube.

3.4 Verification of finite element analysis models

3.4.1 Failure modes

Failure modes of the rebar-penetrated joint in the finite element analysis and the experiment under low cyclic reversed loading are shown in Fig. 11. It is clear that, the failure mode received in the finite element analysis achieves a good agreement with those in the experiment. The collapse of the composite structure is due to the shear fracture of the reinforced gangue concrete beam, but the core region of the joint is not out of work and the collapse is not appeared in the GCFST column. This demonstrates that the rebar-penetrated joint between GCFST column and RGC beam has large stiffness and high strength to maintain the safety and stability of the whole building under the severe earthquake. Owing to the plastic hinge in the RC beam, the composite structure is collapsed with the shear fracture. These meet the design ideas of code for seismic design of buildings (GB5011-2010 2011) that "strong column and week beam, strong connection and week members".

3.4.2 Load-displacement hysteretic curve

In order to verify the feasibility of finite element analysis models created by using ABAQUS and the accuracy of finite element analysis results, finite element analysis results under low cyclic reversed loading are compared and analyzed with experimental results. Fig. 12 shows the

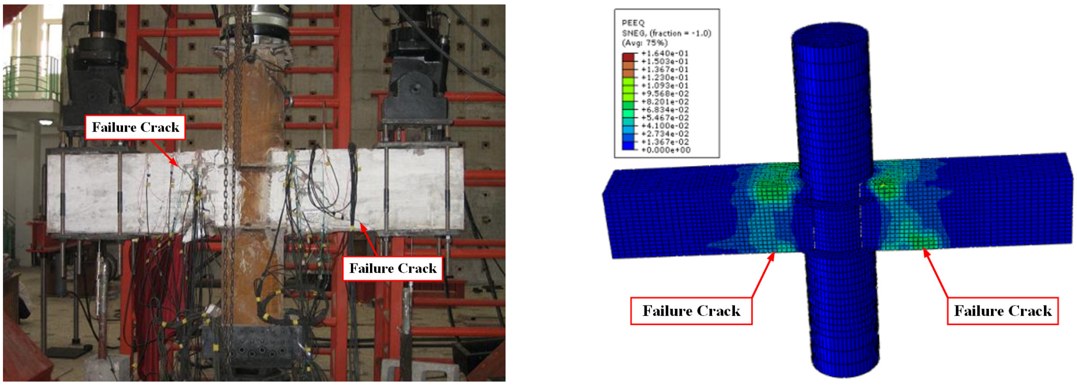

(a) Experiment (b) Finite element analysis

Fig. 11 Failure modes of the rebar-penetrated joint

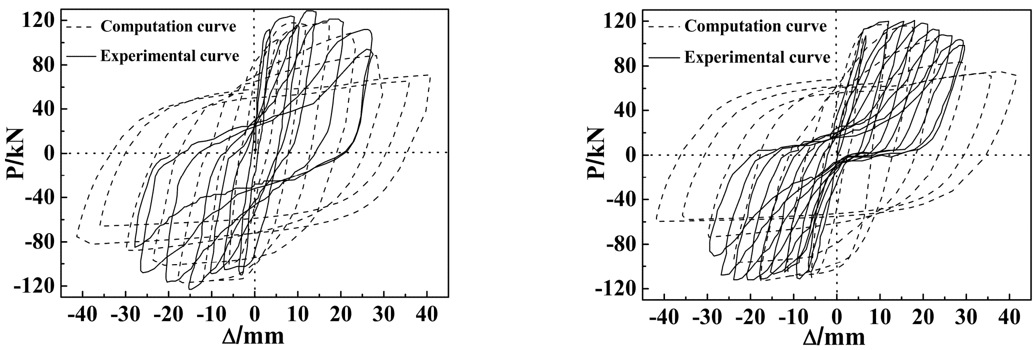

(a) Exterior joint (b) Interior joint

Fig. 12 Comparison between experimental curve and computation curve comparison of load (P)-displacement (Δ) hysteretic curves of the exterior joint and the interior joint between finite element analysis results and experimental results.

From Fig. 12, it is clear that the stiffness and bearing capacity of the joint in the finite element analysis are consistent with the experimental values. However, the experimental curves have the obvious pinch effect phenomenon, while the computation curves are relatively fuller than the experimental curves. So, the shapes of the finite element analysis curves are a little different from experimental curves. But the whole changing trends of finite element analysis curves are accurate and reasonable, which are the same as the experimental curves.

The reasons to result in the difference between finite element analysis curves and experimental curves include: (1) the constitutive model of the gangue concrete used in the paper has some problems in simulating the large bond-slip between rebar and gangue concrete and the crack contact effect of the gangue concrete. At present, few research and analysis are investigated on the constitutive model of gangue concrete. Especially, no studies on the constitutive model of gangue concrete under cyclic loading have been done. However, the crack contact effect of the concrete generated by cyclic load makes a significant influence on the mechanical property of the concrete. Therefore, without the relatively reasonable constitutive model of gangue concrete, it is difficult to make finite element analysis results identical with experimental results. (2) To remedy the defeat of the constitutive model of gangue concrete, the spring model can be used to simulate the bond-slip between rebar and gangue concrete. However, the spring model provided by ABAQUS 6.10 only reflect well the bond-slip under the static loading. Also, the computation convergence is hard to realize with the spring model. As a whole, finite element analysis curves conform well to experimental curves and therefore finite element analysis models are able to complete the research content and purpose.

3.4.3 Skeleton curve

The comparison of skeleton curves of the exterior joint and the interior joint between finite element analysis results and experimental results is shown in Fig. 13. Fig. 13 shows that skeleton curves in finite element analysis are consistent with those in the experiment. The changing trends of finite element analysis curves are the same as experimental curves. Before the peak value of the curve, the curves in finite element analysis are identical with experimental curves. But the values

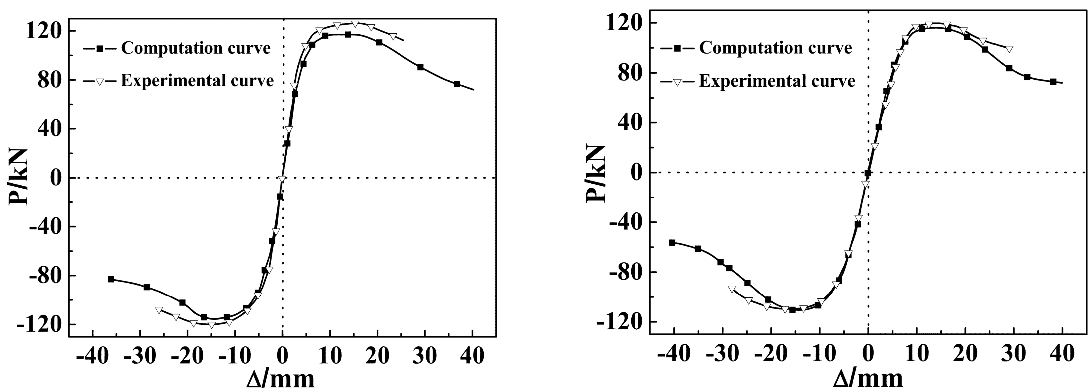

(a) Exterior joint (b) Interior joint

Fig. 13 Comparison between experimental and computation skeleton curves

Table 3 Dimension of the specimen

Specimen label	Column section dimension		Beam section dimension		Longitudinal rebars	N_0 (kN)	n
	$D\times t$ (mm)	H (mm)	$b\times h$ (mm)	L (mm)			
J6-A-B	325×6	1500	240×300	1000	1Φ20	1800	0.6
J6-A-Z	325×6	1500	240×300	2000	1Φ20	1800	0.6
J6-A-0.2	325×6	1500	240×300	2000	1Φ20	600	0.2
J6-A-0.8	325×6	1500	240×300	2000	1Φ20	2250	0.8

in the finite element analysis are less than experimental values after the ultimate bearing capacity. It is due to the constitutive model of gangue concrete and tie model used to connect the different steel components. Tie model provided by ABAQUS 6.10 has some flaws in simulating the performance of the connection under cyclic loading.

As a result, the finite element analysis model created in the research is accurate and reasonable to be the effective complement of the experiment. With finite element analysis models, we make up for the lack of experimental specimens and further analyze the seismic behavior of the rebar-penetrated joint between GCFST column and RGC beam. In the research, finite element analysis models with different axial load levels are conducted by ABAQUS 6.10 to investigate the effect of the axial load level on the seismic behavior of the rebar-penetrated joint and make a comprehensive understanding on the seismic performance of the rebar-penetrated joint. Table 3 shows the dimensions of the models created in the research. In the table, J6-A-B and J6-A-Z have the identical dimensions and material properties with J6-E-B and J6-E-Z to determine the accuracy of the finite element analysis models. For models of J6-A-0.2 and J6-A-0.8, the axial load is changed to create the models with different axial load levels.

4. Analysis and results

4.1 Vertical load-vertical displacement hysteretic curves

The vertical load-vertical displacement hysteretic curves of the specimens are shown in Fig. 14. It is clear that, the rebar-penetrated joint works in the elastic stage at the beginning of testing. The vertical load is approximately proportional to the vertical displacement before the crack is shown in the RGC beam. The vertical load and the vertical displacement increase linearly and the cracks are not formed in the RGC beam. As the cyclic load in the ends of both beams increases, the longitudinal rebar is yielded at the yield strength. The cracks are appeared in the RGC beam and the curve has an obvious inflection point. At the point, the rebar-penetrated joint enters into the elastic-plastic stage, indicating that the load-displacement curves present the more predominant inelastic behavior. The deformation of the joint increases clearly. The cracks in the beams are developing and expanding. In the curves, it is clear to observe the apparent rigidity and strength degradation of the joint. Then, the slope of the curve reduces gradually with the increase of the cyclic load. After the ultimate state, the extent of the decrease is more obvious and the rigidity and strength of the joint are degenerated more significantly owing to the rapid fracture of the gangue concrete. In the meantime, after the ultimate state, the deformation of the joint increases rapidly and the bearing capacity of the joint reduces gradually. It is also obvious that the seismic behavior

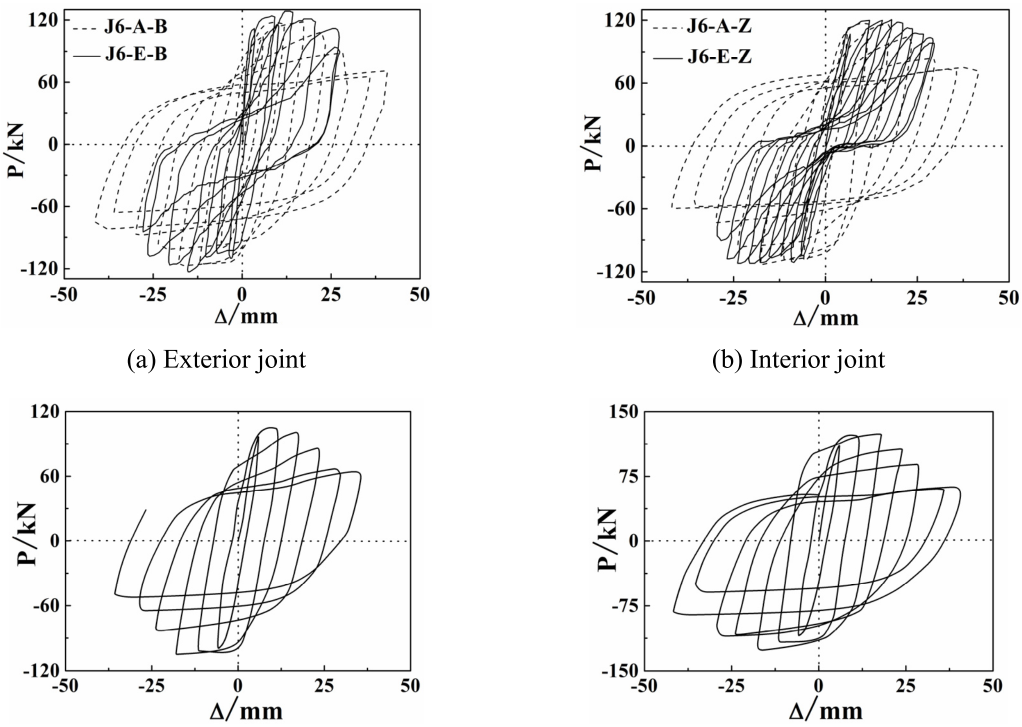

(a) Exterior joint (b) Interior joint

(c) J6-A-0.2 (d) J6-A-0.8

Fig. 14 Vertical load-vertical displacement hysteretic curves

of the joint becomes better with the increase of the axial load level, demonstrating that the axial load can prevent the fractures of the concrete from developing to a certain extent. Therefore, the vertical load-vertical displacement hysteretic curve in the research has the following basic characteristics:

(1) In the initial stage, the load-displacement hysteretic curve increases linearly and the joint works in the elastic stage. With the increase of the cyclic load in ends of both beams, the joint enters into elastic-plastic state and the vertical load is approximately proportional to the vertical displacement. After the ultimate state, the deformation of the joint increases and the bearing capacity reduces gradually.
(2) All vertical load-vertical displacement hysteretic curves are full and spindle-shaped with the different axial load levels. The rigidity and strength degeneration of the joint are more significant after the ultimate bearing capacity. It is due to the fracture of the gangue concrete. These demonstrate that the rebar-penetrated joint between GCFST column and GC beam possesses the excellent seismic performance.

4.2 Bearing capacity

The unified standard has not been proposed and conducted to determine the yield load and failure load for the joint between GCFST column and RGC beam. Therefore, the method proposed

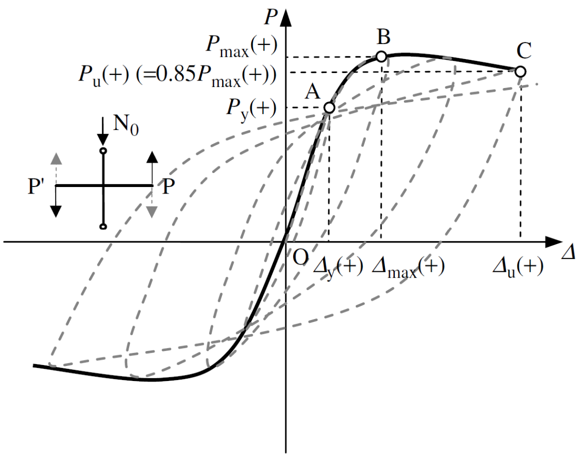

Fig. 15 Typical P-Δ skeleton curve

in the JGJ101-96 code to define the yield strength and the yield displacement of the concrete member is adopted in the research. The typical P-Δ skeleton curve of the joint between column and beam is shown in Fig. 15. The point A corresponds to the initial yielding of the specimen when the longitudinal rebar embedded in the RGC beam is yielded. The yield displacement (Δ_y) is defined as the displacement corresponding to the yield load (P_y). The point B presents the ultimate load (P_{max}) of the joint and the displacement corresponding to the ultimate load is defined as the ultimate displacement (Δ_{max}). The failure load (P_u) is defined as 85% of the ultimate load, which is defined as the point C. The failure displacement (Δ_u) is the displacement corresponding to the failure load.

Table 4 shows critical displacements and loads of the rebar-penetrated joint between GCFST column and GC beam corresponding to points A, B and C. Based on Table 4, it is clear that, (1) the difference of the bearing capacity in each stage between the finite element analysis and the experiment is less than 10%. Before the ultimate bearing capacity of the joint, the loads and displacements in the finite element analysis are almost same as the values in the experiment. After ultimate bearing capacity, finite element analysis results are slightly less than the experimental results, but the difference is controlled in the reasonable range. (2) With the increase of the axial load level, the bearing capacity of the joint with the axial load level of 0.8 increases by 19% more than the bearing capacity of the joint with axial load level of 0.2 and is 1.05 times larger than that

Table 4 Displacement and load of the joint in each stage

Specimen	N_0 (kN)	n	P_y (kN)	Δ_y (mm)	P_{max} (kN)	Δ_{max} (mm)	P_u (kN)	Δ_u (mm)
J6-E-B	1800	0.6	107.4	5.92	122.53	17.31	104.5	27.61
J6-E-Z	1800	0.6	108.3	5.81	119.83	17.27	99.6	26.57
J6-A-B	1800	0.6	103.11	5.88	116.46	16.88	98.99	26.11
J6-A-Z	1800	0.6	107.15	5.85	117.53	17.15	99.05	25.01
J6-A-0.2	600	0.2	89.54	5.76	105.12	16.76	86.75	24.89
J6-A-0.8	2250	0.8	110.12	5.90	121.76	17.02	103.50	24.96

of the joint with axial load level of 0.6. It is clear that the bearing capacity of the joint is increased with the increase of the axial load level. The axial force is helpful to prevent the fracture of the gangue concrete. (3) As a whole, the yield strength, the ultimate bearing capacity and failure load of the joint increase with the increase of the axial load level. In the meantime, the axial compression ratio has little effects on the yield displacement, the ultimate displacement and the failure displacement.

4.3 Strength degradation

The strength degradation of the joint can be evaluated by the strength degradation coefficient (λ_j) (Han and Yang 2004) at the total loads which is to investigate the decrease of the load during the process of testing and analyze the characteristics of the strength degradation of the joint. The strength degradation coefficient at the total loads is expressed as Eq. (2)

$$\lambda_j = \frac{P_j}{P_{\max}} \tag{2}$$

where P_j is defined as the maximum load under the jth loading cycles when the relative displacement (Δ/Δ_y) in the ends of two beams equals to j; $P_{\max}$ is defined as the maximum bearing capacity of the joint during the whole process of testing.

The strength degradation coefficient at the total load versus the relative beam displacement is shown in Fig. 16. Based on Fig. 16, it is obvious that, (1) the changing trend of the curves and the values in the finite element analysis are almost same as those in the experiment. With the increase of the displacement, the strength degradation in the finite element analysis is a little larger than that in the experiment. This is due to the constitutive models of the materials used in the research. (2) The strength degradation coefficient at the total loads increases gradually with the increase of the relative beam displacement when the relative beam displacement is less than 4. As a whole, the trend of the strength degeneration is more and more unclear with the increase of the axial compression ratio. When the relative beam displacement is larger than 4, the strength degradation coefficient at the total loads reduces gradually with the increase of Δ/Δ_y. After the failure point of

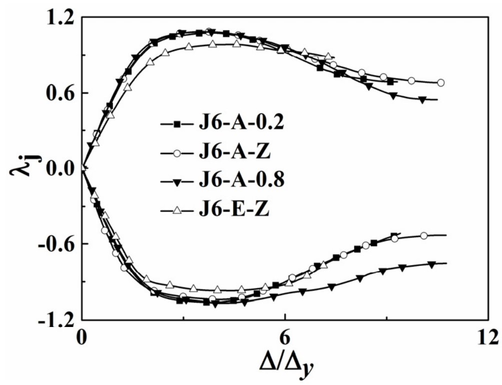

Fig. 16 λ_j-Δ/Δ_y relation curve

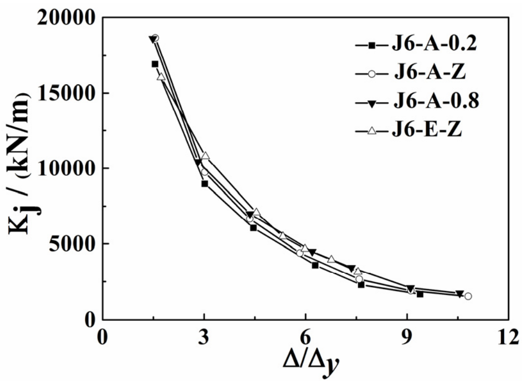

Fig. 17 K_j-Δ/Δ_y relation curve the joint, the curve of the joint has relatively long horizontal part, demonstrating that the joint is able to withstand continuously a large deformation at the failure stage.

4.4 Rigidity degradation

The rigidity is defined as Eq. (3) proposed by Tang (1988).

$$K_j = \frac{\sum_{i=1}^{n} P_j^i}{\sum_{i=1}^{n} u_j^i} \tag{3}$$

where K_j is the rigidity of the joint. P^i_j is defined as the maximum load under the jth loading cycles when the relative displacement (Δ/Δ_y) in the ends of two beams equals to j. u^i_j as the maximum displacement under the jth loading cycles when the relative displacement (Δ/Δ_y) in the ends of two beams equals to j. n is defined as the cycle time of loading.

The rigidity (K_j) of the specimen versus the relative beam displacement is shown in Fig. 17. Based on Fig. 17, as a whole, the rigidity degradation of the rebar-penetrated joint is slow, demonstrating that the rebar-penetrated joint has the good ability to resist the lateral sway. In the meantime, with the increase of the axial load level, the rigidity is increased and the speed of the rigidity degradation becomes slow. In the hysteretic curve, the bearing capacity of the joint is reduced after the ultimate load. The strength and rigidity degradation result in the decrease of the bearing capacity of the joint. And the main factors to cause the strength and rigidity degradation are the elastic-plastic property of the joint and the damage accumulation. The damage is primarily resulted from the formation and development of the crack in the concrete. However, owing to the confinement effect of the tube on the gangue concrete, the development of the crack is slowed down and the fracture of the gangue concrete is delayed. Therefore, the confinement effect of the tube reduces the speeds of the strength degradation and the rigidity degradation of the joint.

4.5 Ductility

Ductility is the physical property of the structure where it is capable of sustaining large permanent changes in shape without breaking. In the anti-earthquake design of the composite structure, the ductility is one of essential factors. The ductility of the joint can be evaluated by the displacement ductility coefficient (μ). The displacement ductility coefficient is defined as the ratio between the failure displacement (Δ_u) and the yield displacement (Δ_y), which is formulated as

$$\mu = \frac{\Delta_u}{\Delta_y} \tag{4}$$

Table 5 shows the displacement ductility coefficients of the rear-penetrated joint specimens. Fig. 18 shows the effect of the axial load level on the ductility of the rebar-penetrate joint. Based on Table 3, it is clear that, (1) the displacement ductility coefficient of the test specimens are in the range of 4.2~4.4, which meet the basic anti-earthquake design principle proposed by Tang (1988) in China that the displacement ductility coefficient of the reinforced concrete structure should be equal to or larger than 3. Therefore, the rebar-penetrated joint between GCFST column and RGC beam displays excellent ductility and can meet the requirement of the seismic design. (2) Based on

Table 5 Ductility coefficient

Specimen	n	Δ_y/mm	Δ_u/mm	μ
J6-E-B	0.6	5.92	27.61	4.66
J6-E-Z	0.6	5.81	26.57	4.57
J6-A-B	0.6	5.88	26.11	4.44
J6-A-Z	0.6	5.85	25.01	4.28
J6-A-0.2	0.2	5.76	24.89	4.32
J6-A-0.8	0.8	5.90	24.96	4.23

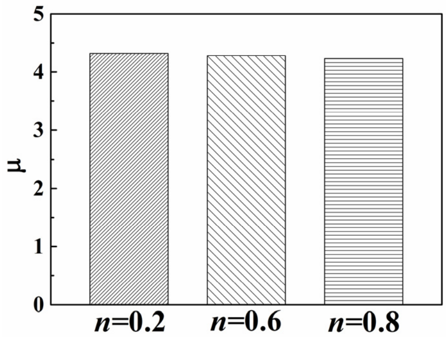

Fig. 18 Effect of n on ductility

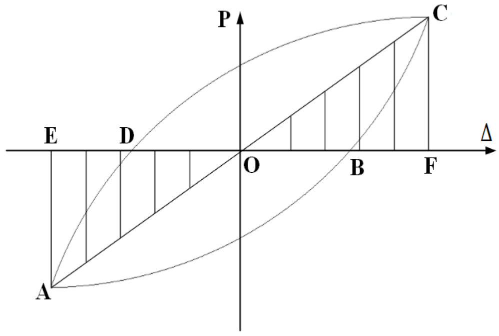

Fig. 19 Equivalent viscous damping coefficient

Fig. 11 and Table 5, with the increase of the axial load level, the ductility of the joint is reduced slightly, but the axial load level makes a small effect on the ductility of the joint.

According to Fig. 19 and Table 5, the ductility of the joint with ring beam is reduced slightly with the increase of axial load level, demonstrating that the increase of the axial load is helpful for the composite structure to improve the ductility.

4.6 Energy dissipation

The equivalent damping coefficient and the energy dissipation coefficient recommended by "Specification of testing methods for earthquake resistant building" are used to analyze the energy dissipation ability of the rebar-penetrated joint between GCFST column and GC beam. The vertical load (P)-deflection (Δ) hysteretic relationship may be described as shown in Fig. 19. According to Fig. 19, the equivalent damping coefficient (h_e), from the simplification, is formulate as Eq. (5)

$$h_e = \frac{1}{2\pi}\frac{S_{ABD}+S_{BCD}}{S_{OAE}+S_{OCF}} \tag{5}$$

where S_{ABD} and SB_{CD} are the area enclosed by the curve ABD and the curve BCD, respectively. S_{OAE} and S_{OCF} are the area enclosed by the curve OAE and the curve OCF, prospectively. The energy dissipation coefficient is defined as the ratio of the total energy in a hysteretic loop to the elastic energy of the joint, which is expressed as Eq. (6)

Table 6 Energy dissipation coefficients

Specimen	n	h_e	E
J6-E-B	0.6	0.39	2.442
J6-E-Z	0.6	0.382	2.399
J6-A-B	0.6	0.42	2.59
J6-A-Z	0.6	0.41	2.58
J6-A-0.2	0.2	0.40	2.56
J6-A-0.8	0.8	0.47	2.95

$$E = 2\pi \cdot h_e \tag{6}$$

Table 6 shows the equivalent damping coefficient (h_e) and the energy dissipation coefficient (E) of the rebar-penetrated joint specimens. Based on the hysteretic curves of the joint and Table 6, it is clear that, before the ultimate bearing capacity of the joint, the hysteretic curve is full and spindle-shaped, demonstrating that the joint shows the good energy dissipation. After the ultimate bearing capacity, the curve enters into the descent stage and the pinch effect phenomenon are shown in the hysteretic curve. The experimental curves show that the rebar-penetrated joint has the excellent energy dissipation. The equivalent damping coefficients of the rebar-penetrated joint specimens in the research are larger than 0.3 and satisfy the anti-earthquake requirements of the construction in China. While the average damping coefficient for normal reinforced concrete joints is approximately 0.1, the equivalent damping coefficients of all specimens in the research lie in the range of 0.38~0.47. It demonstrates that the energy dissipation ability of the rebar-penetrated joint between GCFST column and RGC beam is better than that of conventional reinforced concrete joint. Moreover, with the increase of the axial load level, the equivalent damping coefficient and the energy dissipation coefficient increase gradually. This demonstrates that, as the axial compression ratio increases, the energy dissipation of the rebar-penetrated joint between GCFST column and RGC beam is improved gradually.

5. Conclusions

In the research, the experiment and the finite element analysis are conducted to investigate the seismic behavior of the rebar-penetrated joint between GCFST column and RGC beam. The bearing capacity, the ductility, the strength and rigidity degradation and the energy dissipation of the rebar-penetrated joint are analyzed in details. The following conclusions can be drawn:

- The rebar-penetrated joint between GCFST column and GC beam, with the full and spindle-shaped hysteretic curve, shows the reasonable strength and rigidity degradation, demonstrating that the rebar-penetrated joint possessed the excellent seismic behavior.
- The displacement ductility coefficients of all specimens in the research are larger than 4, which satisfies the requirement that the displacement ductility coefficient is equal to or larger than 3. The equivalent damping coefficients of all specimens are larger than 0.3 which meet the anti-earthquake requirements of the construction in China. Therefore, the research results show that the rebar-penetrated joint is a prospective structure to be used in

the projects. In addition, the energy-dissipation capacity of the rebar-penetrated joint is improved with the increase of the axial load level.

- The rebar-penetrated joint between GCFST column and RGC beam failed in the beams due to the plastic hinges meeting the codes of the seismic design in China, that "strong column and week beam". This demonstrates that the rebar-penetrated joint is adoptable in the building structures for the anti-earthquake purpose.

Acknowledgments

This project was supported by Liaoning Science Fund (201102177), Technology Program of Ministry of Housing and Urban-Rural Development (2011-k3-23), Liaoning Talents Program (LR2011014).

References

Boger, R.K. (2006), "Non-Monotonic strain hardening and its constitutive representation", Ph.D. Dissertation, The Ohio State University, OH, USA.

CECS28:2012 (2012), *Technical Specification for Concrete-Filled Steel Tubular Structures*, Beijing, China.

Chen, J., Wang, Z. and Wang, J. (2004), "Research on the stiffness of concrete filled tubular column and steel beam joint with stiffening ring", *J. Build. Struct.*, **25**(4), 43-49.

Choi, S., Hong, S. and Kim, Y. (2006), "Modeling analytical moment-rotation curves of semi-rigid connections for CFT square columns and steel beams", *Adv. Struct. Eng.*, **9**(5), 697-706.

Fu, Z., Ji, B., Lv, L. and Zhou, W. (2011), "Behavior of lightweight aggregate concrete filled steel tubular slender columns under axial compression", *Adv. Steel Construct.*, **7**(2), 144-156.

GB5011-2010 (2011), *Code for Seismic Design of Structures*, Beijing, China.

GB50010-2010 (2011), *Code for Design of Concrete Structures*, Beijing, China.

GB50017-2003 (2004), *Code for Design of Steel Structures*, Beijing, China.

GB/T228-2002 (2003), *Metallic Materials--Tensile Testing at Ambient Temperature*, Beijing, China.

GB/T50081-2002 (2003), *Standard for Test Method of Mechanical Properties on Ordinary Concrete*, Beijing, China.

Guo, J. (2011), "Experimental research on performances of concrete with coal gangue", *Proceedings of 2011 International Conference on Materials for Renewable Energy & Environment* (*ICMREE*), Shanghai, China, May.

Han, L. (2000), *Concrete Filled Steel Tubular Structures*, Science Press, Beijing, China.

Han, L. and Huo, J. (2003), "Concrete-filled hollow structural steel columns after exposure to ISO-834 fire standard", *J. Struct. Eng.*, **129**(1), 68-78.

Han, L. and Yang, Y. (2004), *Modern Technique of Concrete Filled Tubular Structure*, China Building Industry Press, Beijing, China.

Han, L., Tao, Z. and Liu, W. (2001), "Concrete-filled steel tubular structures − theory and practice", *J. Fuzhou Univ.* (*Natural Sciences Edition*), **6**, 003.

Hu, H., Huang, C. and Chen, Z. (2005), "Finite element analysis of CFT columns subjected to an axial compressive force and bending moment in combination", *J. Construct. Steel Res.*, **61**(12), 1692-1712.

JGJ101-96 (1997), *Specification of Testing Methods for Aseismic Property of Building*, China Building Industry Press, Beijing, China.

Krawinkler, H. (1978), "Shear in beam-column joints in seismic design of steel frames", *Eng. J.*, **15**(3), 82-91.

Li, G. and Zhao, B. (2003), "Analysis of deflecting process of gangue concrete-filled steel tubular member

under moment", *Steel Construct*., **1**, 006.
Li, G., Shu, Z. and Zhang, C. (2010), "Finite element analysis of gangue concrete-filled steel tubular beam-columns", *J. Shenyang Jianzhu Univ*. (*Natural Science*), **26**(6), 1052-1057.
Li, G.C., Fang, C. and Yu, H.P. (2012), "Finite analysis on performance of joint between gangue concrete filled steel tubular column with through rebar and gangue concrete beam under the monotonic loading", *Appl. Mech. Mater*., **204**, 3724-3730.
Lu, X., Ye, L. and Miu, Z. (2009), *Static-Plastic Analysis on Seismic Performance of the Structure*, China Building Industry Press, Beijing, China.
Sorenson, H.K. (2003), *ABAQUS version 6.4*: *Theory manual*, *users' manual*, *verification manual and example problems manual*, Hibbitt, Karlson, Sorenson Inc., USA.
Sun, Y.X. and Li, X.D. (2011), "Development and design of coal gangue concrete filling material", *Adv. Mater. Res*., **295**, 1198-1201.
Tang, J. (1988), "Seismic design for connection in reinforced concrete frame", *Ind. Construct*., **3**, 011.
U.S. Environment Protection Agency (2009), Green buidling basic information. http://www.epa.gov/greenbuilding/pubs/about.htm.
Varma, A.H., Ricles, J.M., Sause, R. and Lu, L.-W. (2002), "Seismic behavior and modeling of high-strength composite concrete-filled steel tube (CFT) beam-columns", *J. Construct. Steel Res*., **58**(5-8), 725-758.
Yao, G., Chen, Y. and Lin, S. (2010), "Finite element analysis on a new-type of concrete-filled steel tube column-RC beam joint", *Special Structures*, **27**(6), 34-38.
Yao, G., Chen, Y., Huang, Y., Pan, D., Zheng, X. and Xu, W. (2011), "Experimental study on seismic performance of a new-type of concrete-filled steel tube column-RC beam joint", *Ind. Construct*., **41**(2), 97-101.
Yu, T., Teng, J., Wong, Y. and Dong, S. (2010), "Finite element modeling of confined concrete-II: Plastic-damage model", *Eng. Struct*., **32**(3), 680-691.
Zhang, J. and Cao, S. (2009), "Research on the stress-strain curves of structural lightweight aggregate concrete", *Build. Sci*., **24**(11), 83-85.
Zhong, S. (2003), *Concrete Filled Steel Tubular Structures*, Tsinghua University Press, Beijing, P.R. China.

CC